Inverse Power Law Scaling of Energy Dissipation Rate in Nonequilibrium Reaction Networks

Qiwei Yu,[1] Dongliang Zhang,[1] and Yuhai Tu[2]
[1]School of Physics, Peking University, Beijing 100871, China
[2]IBM T. J. Watson Research Center, Yorktown Heights, New York 10598, USA

(Received 13 July 2020; accepted 11 January 2021; published 23 February 2021)

The energy dissipation rate in a nonequilibrium reaction system can be determined by the reaction rates in the underlying reaction network. By developing a coarse-graining process in state space and a corresponding renormalization procedure for reaction rates, we find that energy dissipation rate has an inverse power-law dependence on the number of microscopic states in a coarse-grained state. The dissipation scaling law requires self-similarity of the underlying network, and the scaling exponent depends on the network structure and the probability flux correlation. Existence of the inverse dissipation scaling law is shown in realistic biochemical systems such as biochemical oscillators and microtubule-kinesin active flow systems.

DOI: 10.1103/PhysRevLett.126.080601

Living systems are far from equilibrium. Energy dissipation is critical not only for growth and synthesis but also for more subtle information processing and regulatory functions. The free energy dissipation is directly related to the violation of detailed balance—a hallmark of nonequilibrium systems—in the underlying biochemical reaction networks [1]. In particular, driven by energy dissipation [e.g., adenosine triphosphate (ATP) hydrolysis], these biochemical systems can reach nonequilibrium steady states (NESS) that carry out the desired biological function. One of the fundamental questions is how much energy dissipation is needed for performing certain biological function. Indeed, much recent research has been devoted to understanding the relation between energy cost and performance of biological functions such as sensing and adaptation [2,3], error correction [4,5], and accurate timing in biochemical oscillations [6] and synchronization [7].

Quantitatively, the free energy dissipation rate can be determined by computing the entropy production rate in the underlying stochastic reaction network given the transition rates between all microscopic states of the system [8,9]. However, for complex systems with a large number of microscopic states, the system may only be measured at a coarse-grained level with coarse-grained states and coarse-grained transition rates among them. By following the same procedure for computing entropy production rate, we can determine the energy dissipation rate at the coarse-grained level. Although it is known that coarse graining reduces entropy production [10,11], the quantitative relation between the coarse-grained energy dissipation rate and the "true" dissipation rate obtained at the microscopic level remains elusive. Here, we connect dissipation at different scales by developing a coarse-graining procedure inspired by the real space renormalization group (RG) approach by Kadanoff [12,13] and applying it to various reaction networks in the general state space, which include both physical and chemical state variables. We find that the energy dissipation rate follows an inverse power law dependence on the coarse-graining scale in a wide range of nonequilibrium systems, including microtubule-kinesin active flow systems [14] and biochemical oscillators [15,16].

Nonequilibrium reaction network and dissipation rate.—Each node in a reaction network represents a state of the system and each link represents a reaction with the transition rate from state i to state j given by

$$k_{i,j} = k^0_{i,j}\gamma_{i,j} = \frac{2k_0}{1+\exp(\Delta E_{i,j}/k_BT)}\gamma_{i,j}, \tag{1}$$

where $k^0_{i,j}$ represents the equilibrium reaction rates and $\Delta E_{i,j}(=E_i - E_j)$ is the energy difference between states i and j. We set $k_0 = 1$ for the timescale and $k_BT = 1$ for the energy scale. The equilibrium rates satisfy detailed balance $k^0_{i,j}/k^0_{j,i} = e^{-\Delta E_{i,j}}$ and $\gamma_{i,j}$ represents the nonequilibrium driving force. For a given loop $(l_1, l_2, \ldots, l_n, l_1)$ of size n $(l_{n+1} = l_1)$ in the network, we define a nonequilibrium parameter Γ as the ratio of the product of all the rates in one direction over that in the reverse direction: $\Gamma = \Pi_{k=1}^{n}[(\gamma_{l_{k+1},l_k})/(\gamma_{l_k,l_{k+1}})]$. The system breaks detailed balance if there is one or more loops for which $\Gamma \neq 1$. The steady-state probability distribution $\{P^{ss}_i\}$ can be solved from the master equation: $\sum_j (k_{j,i}P^{ss}_j - k_{i,j}P^{ss}_i) = 0$ with normalization $\sum_i P^{ss}_i = 1$. The steady-state dissipation (entropy production) rate is given by [8,9]

$$\dot{W} = \sum_{i<j}(J_{i,j} - J_{j,i})\ln\frac{J_{i,j}}{J_{j,i}}, \tag{2}$$

where $J_{i,j} = k_{i,j}P_i^{ss}$ is the steady-state probability flux from state i to state j.

State space renormalization and dissipation scaling.—The network can be coarse grained by grouping subsets of highly connected (neighboring) states to form a coarse-grained (CG) state while conserving both total probability of the state and the total probability flux between states. For example, when we group two sets of microscopic states, $(i_1, i_2, \ldots, i_r)$ and $(j_1, j_2, \ldots, j_r)$, to form two CG states i and j, the probability of each CG state is the sum of the probability of all constituent states,

$$P_i^{ss} = \sum_{\alpha=1}^{r} P_{i_\alpha}^{ss}, \qquad P_j^{ss} = \sum_{\alpha=1}^{r} P_{j_\alpha}^{ss}. \tag{3}$$

The transition rates in the CG system is renormalized to preserve the total probability flux from state i to j,

$$k_{i,j} = \frac{J_{i,j}}{P_i^{ss}} = \frac{1}{P_i^{ss}} \sum_{(\alpha,\beta)} J_{i_\alpha,j_\beta} = \frac{\sum_{(\alpha,\beta)} k_{i_\alpha,j_\beta} P_{i_\alpha}^{ss}}{\sum_{\alpha=1}^{r} P_{i_\alpha}^{ss}}. \tag{4}$$

Figure 1(a) demonstrates an example in a square lattice with $r = 4$. The red links correspond to transitions that survive the coarse-graining process with their reaction rates renormalized according to Eq. (4). The black links represent internal transitions that are averaged over during coarse graining. The dissipation rate of the CG system can be computed from Eq. (2) with the renormalized probability distribution [Eq. (3)] and transition rates [Eq. (4)].

For a microscopic system with n_0 states, coarse graining s times leads to a system with n_s states. Each state in the CG system hence contains n_0/n_s original states. We define n_0/n_s as the block size, which is used to characterize the degree (scale) of coarse graining. Our main result is that the dissipation rate of the CG system $\dot{W}(n_s)$ scales as an inverse power law with respect to the block size for a diverse class of reaction networks,

$$\frac{\dot{W}(n_s)}{\dot{W}(n_0)} = \left(\frac{n_0}{n_s}\right)^{-\lambda}, \tag{5}$$

where λ is the dissipation scaling exponent. Furthermore, the exponent λ depends on the structure of the network with an unifying expression for the networks we studied,

$$\lambda = d_L - \log_r(1 + C^*), \tag{6}$$

where $r = n_s/n_{s+1}$ is the number of fine-grained states in a next-level CG state, and the link exponent d_L is defined as the scaling exponent of the total number of links (reactions) L with respect to the block size,

$$d_L \equiv \frac{\ln[L(n_s)/L(n_0)]}{\ln(n_s/n_0)}. \tag{7}$$

C^* is the average correlation between probability fluxes defined as

$$C^* = \frac{\langle A_{i_\alpha,j_\beta}(A_{i,j} - A_{i_\alpha,j_\beta})\rangle_{i_\alpha,j_\beta}}{\sqrt{\langle A_{i_\alpha,j_\beta}^2\rangle_{i_\alpha,j_\beta}\langle(A_{i,j} - A_{i_\alpha,j_\beta})^2\rangle_{i_\alpha,j_\beta}}}, \tag{8}$$

where $A_{x,y} = J_{x,y} - J_{y,x}$ is the net flux between states x and y, and $(A_{i,j} - A_{i_\alpha,j_\beta})$ is the sum of other fluxes that are merged with A_{i_α,j_β} during coarse graining. The detailed derivation of Eq. (6) is provided in Sec. I of the Supplemental Material [17].

In the rest of the paper, we demonstrate the energy dissipation scaling in different types of extended networks. For simplicity, we focus on the simplest case with a flat energy landscape ($\Delta E_{i,j} = 0$) and a random nonequilibrium force $\gamma_{i,j}$ that follows a log normal distribution, namely, $\ln(\gamma_{i,j}) \sim \mathcal{N}(\mu, \sigma)$. Other forms of energy landscape and rate distributions are studied without affecting the general scaling results (see Sec. II in the Supplemental Material [17] for details).

Regular lattice.—We first consider a $N_0 \times N_0$ square lattice network, where the coarse graining is done by grouping four ($= 2 \times 2$) neighboring states at one level to create a CG state at the next level iteratively [Fig. 1(a)]. Both transition rates and the overall dissipation evolve as the system is coarse grained. As shown in Fig. 2(a), the renormalized transition rates follow log normal distributions at all CG levels, i.e., $\ln k \sim \mathcal{N}(\mu, \sigma)$, with mean and variance decreasing with the block size [Fig. 2(b)]. Consequently, the dissipation rate also decreases with coarse graining. Remarkably, the dissipation rate decreases with the block size by following a power law [Fig. 2(c), blue circle]. The numerically determined scaling exponent $\lambda_{2D} = 1.35$ suggests that the dissipation rate decreases

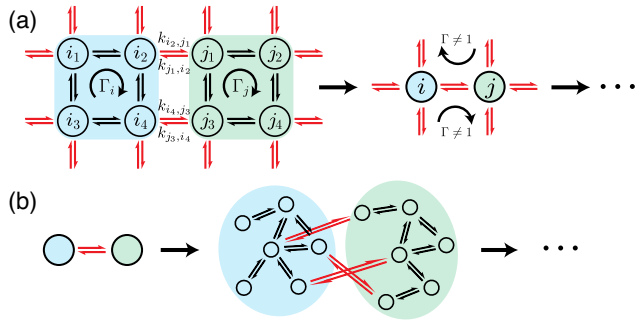

FIG. 1. (a) Illustration of the coarse-graining process in square lattice. All states in the shaded area (blue or green) are merged to form the new CG state. The red links are combined together to form the transition reaction between the new states, while black links correspond to internal transitions that are removed in the CG model. (b) Illustration of the growth mechanism in random hierarchical network. The example here corresponds to $m = 6$, $d = 2$.

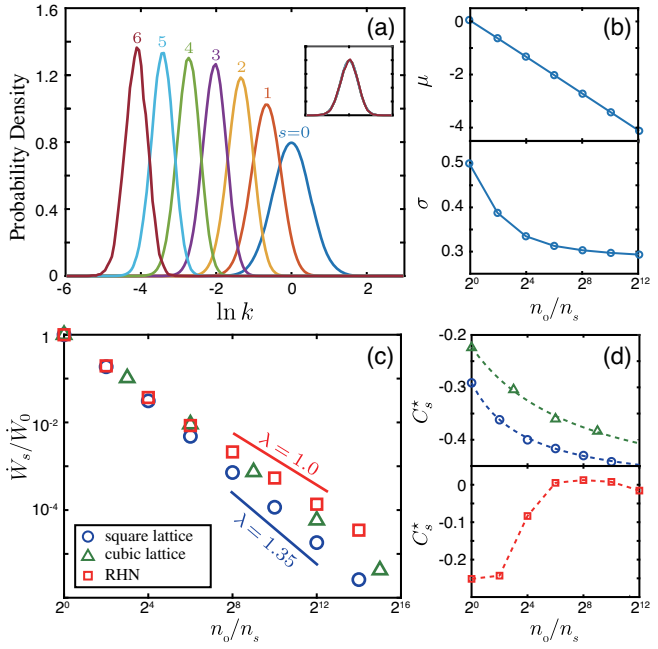

FIG. 2. (a) Probability density function (PDF) of $\ln k_{i,j}$ at different CG levels (from left to right, coarse to fine grained). Inset: normalized PDF all collapse to a standard Gaussian distribution. (b) Mean (μ) and standard deviation (σ) of the $\ln k_{i,j}$ distribution as a function of the block size n_0/n_s. (c) Power-law relation between the scaled dissipation rate $\dot{W}_s/\dot{W}_0$ and the block size n_0/n_s, in square lattice (blue circle), cubic lattice (green triangle), and random hierarchical network (red square, $d = m = 4$). (d) Correlation coefficient C_s^* of the three systems plotted in (c).

faster than the block size. As the number of links is inversely proportional to the block size in a regular lattice, we have $d_L = 1$. According to Eq. (6), the dissipation scaling exponent $\lambda_{2D} = 1 - \log_4(1 + C^*)$, where C^* denotes the probability flux correlation coefficient defined in Eq. (8). C^* can be calculated from direct simulations [Fig. 2(d), blue circles], and it appears to decrease with the block size and converges to a fixed point ~ -0.50 (by extrapolation), which corresponds to a scaling exponent of $\lambda = 1.50$ at the infinite size limit. For the finite systems studied here, the correlation coefficient C^* is larger than its infinite size value, and the exponent found in our simulations is slightly smaller ($\lambda_{2D} = 1.35 < 1.50$).

The 2D results can be generalized to regular lattice in higher dimensions, where $d_L = 1$ and the correlation coefficient C^* converges to a fixed value dependent on the dimension. For example, the numerically determined scaling exponent in the cubic regular lattice is $\lambda_{3D} = 1.23 > 1$ [Fig. 2(c), green triangles] as C^* in 3D is found to converge to a value slightly greater than its 2D value [Fig. 2(d), green triangles).

Random hierarchical network.—To investigate the dissipation scaling behavior in networks with irregular structures, we introduce the random hierarchical networks (RHNs), which share some features of the regular lattice, such as the conservation of average degree at different CG levels. However, links among neighboring states in RHNs are created randomly. A RHN is constructed from a small initial network with n_s states by an iterative growth process. In each growth iteration, each macrostate splits into m microstates with $(md)/4$ links randomly created among them. Each link then splits into $m/2$ links by randomly choosing $m/2$ distinct pairs of microstates that belong to the two macrostates and connecting them pairwise. In this way, the average degree d is preserved in all of the CG levels. Each growth step results in an m-fold increase in both the number of states and the number of links, leading to $d_L = 1$, however, the local reaction links are randomly chosen in RHNs.

The coarse-graining process follows precisely the reversal of the growth procedure. As shown in Fig. 2(c) (red squares), the dissipation rate in RHNs also scales with the block size in a power-law manner with the scaling exponent $\lambda_{RHN} \approx 1$ regardless of the choices of parameters (d and m) used to grow the RHN (see Table S1 in the Supplemental Material [17] for details). In RHNs, the flux correlation C^* vanishes at the RG fixed point [Fig. 2(d), red squares] due to the randomness of reaction links. Therefore, according to Eq. (6), we have $\lambda_{RHN} = d_L = 1$ independent of d or m. The RHN can be considered as a mean-field generalization of a regular lattice of dimension $\log_2 m$. In both cases, the link exponent $d_L = 1$, the different dissipation scaling exponents come from the different flux correlation C^*.

Scaling requires network self-similarity.—We next study how the dissipation scaling depends on topology of the network by considering embedded scale-free networks (SFNs) characterized by a power-law degree distribution $p(k) \propto k^{-\alpha}$ ($k \geq k_{\min}$) [17,23–26]. We find that the dissipation rate in the 2D-embedded SFN also scales with block size as a power law with the exponent λ depending on the link exponent d_L and flux correlation coefficient C^* as given in Eq. (6). Because of the local randomness in SFNs, we expect $C^* \approx 0$ as in RHNs, and d_L depends on the fractal dimension d_B and exponent α of the embedded SFN (see Sec. I in the Supplemental Material [17] for detailed derivation). However, the dissipation scaling relation does not exist in all networks. For example, even though the dissipation rate decreases with coarse graining in both Watts-Strogatz small-world network [27] and the Erdős-Rényi random network [28], the scaling law defined by Eq. (5) is not satisfied in either of these networks (see Fig. S15 in the Supplemental Material [17]). The existence of the dissipation scaling law depends on whether the network has self-similarity, i.e., whether the CG process converges the network to the complete-graph fixed point or a self-similar (fractal) fixed point [29]. The regular lattices, RHNs, and SFNs converge to a self-similar fixed point, i.e., networks at all CG levels are structurally similar and properties like the number of links (reactions) and total

dissipation rate all scale in a power-law fashion. However, in the small-world network or the Erdős-Rényi network, the CG process eventually generates a complete graph with all nodes directly connected.

Dissipation scaling in biochemical systems.—Here, we demonstrate the general dissipation scaling behavior in two biochemical systems with their state variables defined in chemical and physical space, respectively.

(1) The Brusselator model: The Brusselator model describes a class of biochemical systems that can generate sustained oscillations [15,30]. Here, we study the dissipation scaling in the reversible Brusselator model [16] where dynamics of molecules X and Y are given by the following multimolecular chemical reactions:

$$A \underset{k_{-1}}{\overset{k_1}{\rightleftharpoons}} X; \quad B + X \underset{k_{-2}^0}{\overset{k_2^0}{\rightleftharpoons}} D + Y; \quad 2X + Y \underset{k_{-3}}{\overset{k_3}{\rightleftharpoons}} 3X,$$

with constant reaction rates (k's) and constant concentrations for auxiliary molecules A, B, and D. As shown in Fig. 3(a), the chemical state space of the Brusselator model is spanned by two state variables n_x and n_y that represent the number of X and Y molecules, respectively. Different from the random flux model, transition rates in the Brusselator reaction network depend deterministically on the state variables n_x and n_y (see Sec. III in the Supplemental Material [17] for details). In addition, the Brusselator network has diagonal links (reactions) that convert between X and Y molecules. Despite these differences, the same coarse-graining procedure can be applied to study dissipation scaling in the Brusselator model. As shown in Fig. 3(b), dissipation rate of the Brusselator model follows a power-law dependence on the block size with an exponent $\lambda \approx 0.56$.

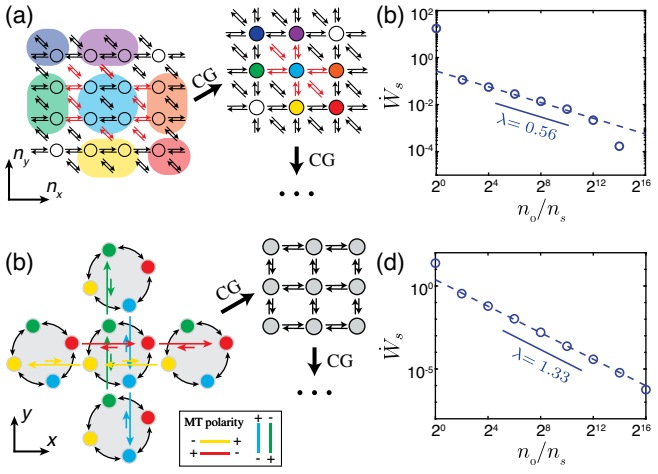

FIG. 3. (a) The reaction network and the coarse-graining scheme for the Brusselator system. The four states in the central blue shade form the new blue state, the red links are coarse grained into the links between the new blue state and adjacent states. (b) The scaling of dissipation rate $\dot{W}_s$ in Brusselator. (c) The reaction network for the microtubule-kinesin mixture. Each gray circle denotes a spatial location, and the four colors denote different MT orientations. (d) The scaling of dissipation rate $\dot{W}_s$ in the MT-kinesin system. See the Supplemental Material [17] for parameters used in (b) and (d).

(2) The microtubule-kinesin system: The state space coarse-graining process and the dissipation scaling analysis can be applied to active matter systems, e.g., a microtubule-kinesin mixture where the active transport of microtubules (MTs) powered by ATP-consuming kinesin can lead to macroscopic flows [14]. To investigate possible dissipation scaling behavior in active transport systems, we developed a simple 2D lattice model for a MT-kinesin mixture, which can be extended to 3D. As shown in Fig. 3(c), the microscopic state variables for a MT molecule are its physical location (i, j) and its polarity $p = 1$–4 [labeled by different colors in Fig. 3(c)], which corresponds to the four possible directions in the 2D model. At each site (i, j), the MT can change its orientation by 90° with a switching rate ω. The transport rate of the MT at site (i, j) in direction p is given by $k_{i,j,p} = k_d + \tilde{k}_{i,j,p}(n_{i,j,p})$, where k_d is a small passive transport rate due to thermal diffusion and $\tilde{k}_{i,j,p}$ is the active transport rate that depends on $n_{i,j,p}$—the number of kinesin motors at site (i, j) that drive the active transport along p direction. Without considering motor-motor interaction, we use the leading order linear dependence: $\tilde{k}_{i,j,p} = k_0 n_{i,j,p}$, where $k_0 (\gg k_d)$ is a large single-kinesin active transport rate that increases with the ATP concentration. To make our model thermodynamically consistent, a reverse rate $k_{i,j,-p} = k_d + \tilde{k}_{i,j,p} \exp(-n_{i,j,p}\Delta\mu_0)$ is included with $\Delta\mu_0$ the free energy dissipation in ATP hydrolysis. For simplicity, we assume that $n_{i,j,p}$ follows an independent identically distributed Gaussian distribution $n_{i,j,p} \sim \max(0, \mathcal{N}(\mu, \sigma))$ [31]. The coarse-graining procedure is applied for the MT-kinesin network. The first iteration combines the four orientation states at the same location, and the subsequent iterations merge neighboring spatial locations. As shown in Fig. 3(d), the dissipation rate in the coarse-grained networks follows a power-law scaling relation with an exponent $\lambda \approx 1.33$ after the initial coarse-graining step. In reality, dynamics of the kinesin number $n_{i,j,p}$, which is coupled with MT dynamics, can lead to spatial correlation in $n_{i,j,p}$. However, the dissipation scaling law remains true when spatial correlation in $n_{i,j,p}$ is introduced (see Sec. III in the Supplemental Material [17] for details).

Discussion.—The dissipation scaling in self-similar reaction networks is reminiscent of the Kolmogorov scaling theory in homogeneous turbulence, which is based on self-similarity of the turbulence structures ("eddies") at different scales in the inertia range [32,33]. However, as illustrated in Fig. 4, while energy is introduced at large length scale in turbulence, free energy is injected at the microscopic scale in reaction networks, which leads to the "inverse cascade" of energy dissipation. Furthermore, while energy

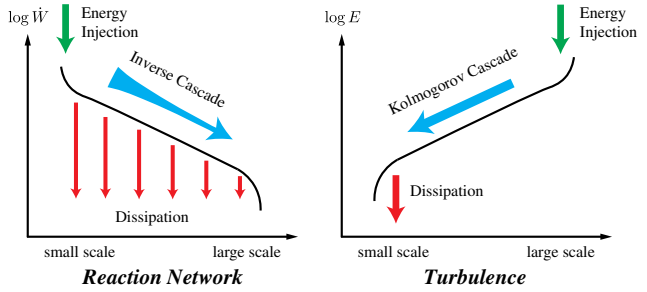

FIG. 4. Comparison between the inverse energy dissipation cascade in self-similar reaction networks and the Kolmogorov energy cascade in turbulence. See text for detailed discussion.

is conserved within the inertia range in turbulence, it is dissipated at all scales in nonequilibrium networks. In fact, the inverse scaling law (5) indicates that the energy dissipation rate in a coarse-grained network (CGN) is much lower than that in its preceding fine-grained network (FGN). The difference in energy dissipation in CGN and FGN is due to two "hidden" free energy costs in CGN: (1) the energy dissipation needed to maintain the NESS of a CG state, which contains many internal microscopic states and transitions among them, and (2) the entropy production due to merging multiple reaction pathways into a CG reaction between two CG states [34,35] (See Sec. IV in the Supplemental Material [17] for details).

The state space coarse-graining approach and the dissipation scaling analysis developed here provide a general framework to study nonequilibrium thermodynamics of biochemical systems where dynamics may only be measured at coarse-grained (mesoscopic) scales [14,36]. In particular, the dissipation scaling relation provides a powerful tool for estimating the true microscopic dissipation rate from mesoscopic measurements. For example, in the MT-kinesin system, ATP is hydrolyzed to drive the relative motion of microtubules with the microscopic coherent length given by the kinesin persistent run length $l_0 \sim 0.6$–1 μm [37,38]. The active flow of the MT-kinesin system can occur at a much larger length scale $l_f \sim 100$ μm [14]. By using the dissipation scaling law [Eq. (5)], the energy dissipation rate $\dot{W}_f$ determined from the flow velocity field at the length scale l_f is orders of magnitude smaller than the true energy dissipation rate $\dot{W}_0$ at the microscopic scale l_0: $(\dot{W}_f/\dot{W}_0) \approx [(l_0/l_f)^3]^{\lambda_{3D}} \approx 10^{-7.4}$–$10^{-8.2}$ where $\lambda_{3D} = 1.23$ for the 3D regular lattice network is used. This means that most of the energy is spent to generate and maintain the flow motion at different length scales from l_0 to l_f, and only a tiny amount is used to overcome viscosity at the large flow scale l_f. It would be interesting to test this large difference in energy dissipation experimentally.

Y. T. acknowledges stimulating discussions with Dr. Dan Needleman and Dr. Peter Foster, whose measurements of heat dissipation in active flow systems partly inspired this work. The work by Y. T. is supported by a NIH Grant No. R35GM131734. Part of this work was finished by Y. T. during a KITP workshop on "Cellular Energetics," for which supports from NSF Grant No. PHY-1748958, NIH Grant No. R25GM067110, and the Gordon and Betty Moore Foundation Grant No. 2919.02 are acknowledged. Q. Y. thanks the hospitality of Center for Theoretical Biological Physics, Rice University.

[1] F. S. Gnesotto, F. Mura, J. Gladrow, and C. P. Broedersz, Broken detailed balance and non-equilibrium dynamics in living systems: A review, Rep. Prog. Phys. **81**, 066601 (2018).
[2] G. Lan, P. Sartori, S. Neumann, V. Sourjik, and Y. Tu, The energy-speed-accuracy trade-off in sensory adaptation, Nat. Phys. **8**, 422 (2012).
[3] P. Mehta and D. J. Schwab, Energetic costs of cellular computation, Proc. Natl. Acad. Sci. U.S.A. **109**, 17978 (2012).
[4] J. J. Hopfield, Kinetic proofreading: A new mechanism for reducing errors in biosynthetic processes requiring high specificity, Proc. Natl. Acad. Sci. U.S.A. **71**, 4135 (1974).
[5] C. H. Bennett, Dissipation-error tradeoff in proofreading, BioSystems **11**, 85 (1979).
[6] Y. Cao, H. Wang, Q. Ouyang, and Y. Tu, The free-energy cost of accurate biochemical oscillations, Nat. Phys. **11**, 772 (2015).
[7] D. Zhang, Y. Cao, Q. Ouyang, and Y. Tu, The energy cost and optimal design for synchronization of coupled molecular oscillators, Nat. Phys. **16**, 95 (2020).
[8] T. L. Hill, *Free Energy Transduction in Biology* (Academic Press, New York, 1977).
[9] H. Qian, Open-system nonequilibrium steady state: Statistical thermodynamics, fluctuations, and chemical oscillations, J. Phys. Chem. B **110**, 15063 (2006).
[10] D. M. Busiello and A. Maritan, Entropy production in master equations and Fokker-Planck equations: Facing the coarse-graining and recovering the information loss, J. Stat. Mech. (2019) 104013.
[11] D. M. Busiello, J. Hidalgo, and A. Maritan, Entropy production for coarse-grained dynamics, New J. Phys. **21**, 073004 (2019).
[12] L. P. Kadanoff, Scaling laws for Ising models near T_c, Phys. Phys. Fiz. **2**, 263 (1966).
[13] K. G. Wilson, The renormalization group: Critical phenomena and the Kondo problem, Rev. Mod. Phys. **47**, 773 (1975).
[14] T. Sanchez, D. T. N. Chen, S. J. DeCamp, M. Heymann, and Z. Dogic, Spontaneous motion in hierarchically assembled active matter, Nature (London) **491**, 431 (2012).
[15] H. Qian, S. Saffarian, and E. L. Elson, Concentration fluctuations in a mesoscopic oscillating chemical reaction system, Proc. Natl. Acad. Sci. U.S.A. **99**, 10376 (2002).
[16] C. Fei, Y. Cao, Q. Ouyang, and Y. Tu, Design principles for enhancing phase sensitivity and suppressing phase fluctuations simultaneously in biochemical oscillatory systems, Nat. Commun. **9**, 1434 (2018).

[17] See Supplemental Material at http://link.aps.org/supplemental/10.1103/PhysRevLett.126.080601 for details of SFN and simulation results, which includes Refs. [18–22].
[18] C. Song, S. Havlin, and H. A. Makse, Self-similarity of complex networks, Nature (London) **433**, 392 (2005).
[19] C. Song, L. K. Gallos, S. Havlin, and H. A. Makse, How to calculate the fractal dimension of a complex network: The box covering algorithm, J. Stat. Mech. (2007) P03006.
[20] J. S. Kim, K.-I. Goh, B. Kahng, and D. Kim, Fractality and self-similarity in scale-free networks, New J. Phys. **9**, 177 (2007).
[21] L. Fenton, The sum of log-normal probability distributions in scatter transmission systems, IRE transactions on communications systems **8**, 57 (1960).
[22] R. L. Mitchell, Permanence of the log-normal distribution, J. Opt. Soc. Am. **58**, 1267 (1968).
[23] A.-L. Barabási and R. Albert, Emergence of scaling in random networks, Science **286**, 509 (1999).
[24] A.-L. Barabási, Scale-free networks: A decade and beyond, Science **325**, 412 (2009).
[25] A. F. Rozenfeld, R. Cohen, D. ben-Avraham, and S. Havlin, Scale-Free Networks on Lattices, Phys. Rev. Lett. **89**, 218701 (2002).
[26] B. J. Kim, Geographical Coarse Graining of Complex Networks, Phys. Rev. Lett. **93**, 168701 (2004).
[27] D. J. Watts and S. H. Strogatz, Collective dynamics of "small-world" networks, Nature (London) **393**, 440 (1998).
[28] P. Erdős and A. Rényi, On random graphs I., Publ. Math. (Debrecen) **6**, 290 (1959).
[29] H. D. Rozenfeld, C. Song, and H. A. Makse, Small-World to Fractal Transition in Complex Networks: A Renormalization Group Approach, Phys. Rev. Lett. **104**, 025701 (2010).
[30] G. Nicolis and I. Prigogine, *Self-Organization in Non-Equilibrium Systems* (Wiley, New York, 1977).
[31] Other forms of distribution have been used without affecting the results.
[32] S. B. Pope, *Turbulent Flows* (Cambridge University Press, Cambridge, England, 2000).
[33] Z. Warhaft, Passive scalars in turbulent flows, Annu. Rev. Fluid Mech. **32**, 203 (2000).
[34] M. Santillán and H. Qian, Irreversible thermodynamics in multiscale stochastic dynamical systems, Phys. Rev. E **83**, 041130 (2011).
[35] M. Esposito, Stochastic thermodynamics under coarse graining, Phys. Rev. E **85**, 041125 (2012).
[36] C. Battle, C. P. Broedersz, N. Fakhri, V. F. Geyer, J. Howard, C. F. Schmidt, and F. C. Mackintosh, Broken detailed balance at mesoscopic scales in active biological systems, Science **352**, 604 (2016).
[37] R. D. Vale, T. Funatsu, D. W. Pierce, L. Romberg, Y. Harada, and T. Yanagida, Direct observation of single kinesin molecules moving along microtubules, Nature (London) **380**, 451 (1996).
[38] S. Verbrugge, S. M. Van Den Wildenberg, and E. J. Peterman, Novel ways to determine kinesin-1's run length and randomness using fluorescence microscopy, Biophys. J. **97**, 2287 (2009).